UCRL-JC-124701
PREPRINT

Large-Eddy Simulation in Complex Domains using the Finite Element Method

R. C. McCallen
B. T. Kornblum
W. Kollman

This paper was prepared for submittal to the
1997 American Society of Mechanical Engineers
Fluids Engineering Division Summer Meeting
Vancouver, British Columbia, Canada
June 22-26, 1997

November 12, 1996

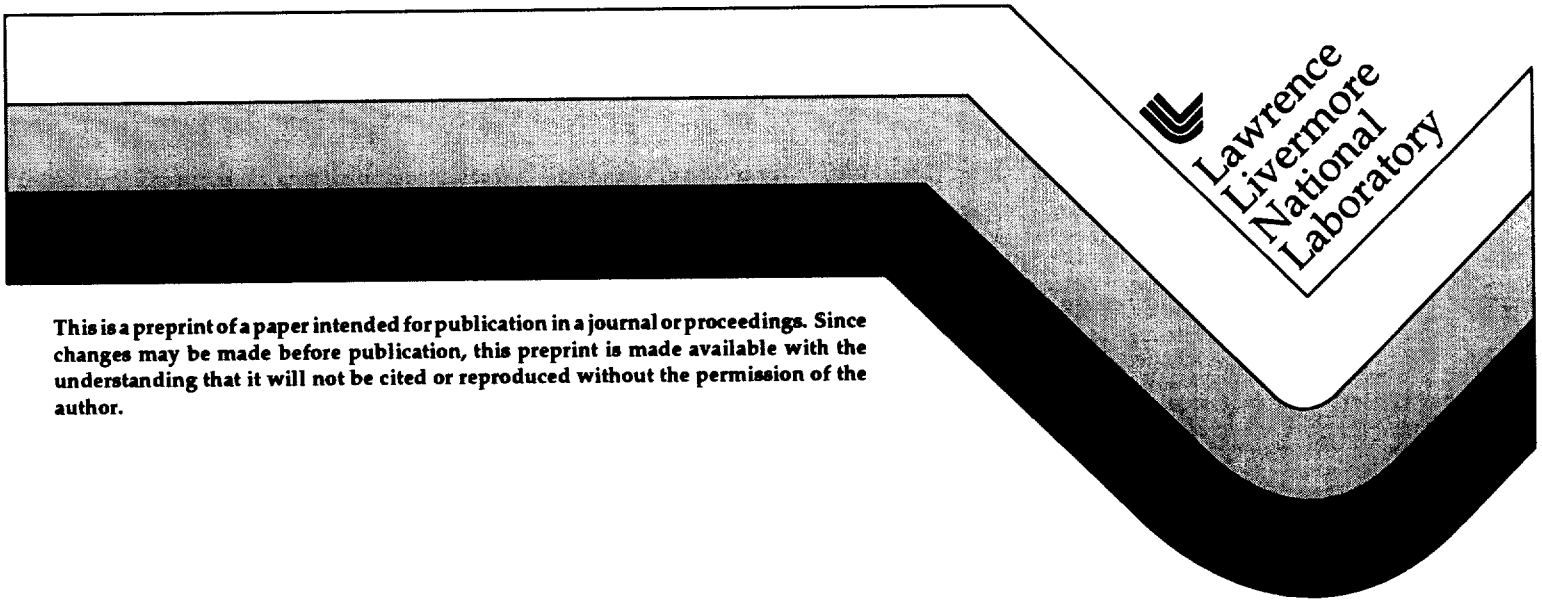

LARGE-EDDY SIMULATION IN COMPLEX DOMAINS USING THE FINITE ELEMENT METHOD

Rose C. MCCALLEN and Barbara T. KORNBLUM

Lawrence Livermore National Laboratory, University of California, Livermore, CA 94551, USA

W. KOLLMANN

MAE Dept., University of California, Davis, CA.95616, USA

Abstract

Large-eddy simulation for the modeling of turbulent flow is used in conjunction with the finite element method. This approach is shown to accurately predict the transient, complex flow over a three-dimensional backward-facing step at a Reynolds number of 10,000. The instantaneous and time-averaged results for the large-eddy simulation are evaluated by comparison to a direct numerical simulation. In addition, the three-dimensional LES results are compared to experimental results.

1 Introduction

In a large-eddy simulation (LES) of turbulent flows, the large-scale motion is calculated explicitly (i.e., resolved) and the small-scale motion is modeled (i.e., approximated with semi-empirical relations). Typically, finite difference or spectral numerical schemes are used to generate an LES; the use of finite element methods (FEM) has been far less common.

Few publications have appeared in the open literature where LES was combined with FEM for the simulation of incompressible flows (Kondo et al. [1], Findikakis et al. [2], Findikakis and Street [3]). Kondo et al. [1] simulated the coupled fluid/structure problem of turbulent flow past an elastic shell. Findikakis et al. [2] and Findikakis and Street [3] simulated turbulent stratified flows with a free surface representative of reservoirs, lakes, and estuaries.

In this study, we demonstrate that FEM in combination with LES provides a viable tool for the study of turbulent, separating channel flows, specifically the flow over a backward-facing step. The combination of these methodologies brings together the advantages of each; LES provides a high degree of accuracy with a minimum of empiricism for turbulence modeling and FEM provides a robust way to simulate flow in very complex domains of practical interest. Such a combination should prove very valuable to the engineering community.

2 Governing equations and FEM formulation

The LES averaging of the instantaneous velocity for all the turbulent motions, $u_\alpha(\underline{x},t)$, filters out the small-scale motions, $u'_\alpha(\underline{x},t)$, and results in the instantaneous velocity for only the large-scale motions, $\overline{u}_\alpha(\underline{x},t)$, such that $u_\alpha = \overline{u}_\alpha + u'_\alpha$ holds. The overbar represents a filtering operator (Kwak et al., 1975 [4]) defined by

$$\overline{u}_\alpha(\underline{x},t) \equiv \int_\Omega d\underline{x}' G(\underline{x},\underline{x}') u_\alpha(\underline{x}',t) \tag{1}$$

where G denotes the filter function normalized to unity and Ω denotes the flow domain. The large-scale motions which are explicitly computed are called the resolved field, and the small-scale motions which are modeled are called the subgrid-scale (SGS) motion or residual field. For finite domains Ω, the resolved field can be defined by the top hat filter function in (1), equivalent to volume averaging,

$$G(\underline{x},\underline{x}') = \begin{cases} \frac{1}{V(\underline{x})} & \text{for } \underline{x}' \in \Omega_G(\underline{x}) \\ 0 & \text{otherwise} \end{cases} \tag{2}$$

where $\Omega_G(\underline{x}) \subset \Omega$ denotes the filter support, which may be a grid cell or finite element containing the point $\underline{x}$, and $\mathcal{V}(\underline{x})$ its volume. The filtered incompressible Navier-Stokes equations are [6] then:

$$\frac{\partial \overline{u}_\alpha}{\partial x_\alpha} = 0 \tag{3}$$

$$\frac{\partial \overline{u}_\alpha}{\partial t} + \frac{\partial}{\partial x_\beta}(\overline{u}_\alpha \overline{u}_\beta) = \frac{\partial}{\partial x_\beta}\overline{\tau}_{\alpha\beta} \tag{4}$$

where the pseudo-stress term is

$$\overline{\tau}_{\alpha\beta} = -\overline{P}\delta_{\alpha\beta} + \nu\frac{\partial \overline{u}_\alpha}{\partial x_\beta} - (R_{\alpha\beta} + D_{\alpha\beta} + L_{\alpha\beta}) \tag{5}$$

where

$$P = \frac{\overline{p}}{\rho} + \frac{1}{3}\overline{u'_\alpha u'_\alpha} \tag{6}$$

and

$$L_{\alpha\beta} = \overline{\overline{u}_\alpha \overline{u}_\beta} - \overline{u}_\alpha \overline{u}_\beta \tag{7}$$

$$C_{\alpha\beta} = \overline{u'_\alpha \overline{u}_\beta} + \overline{\overline{u}_\alpha u'_\beta} \tag{8}$$

$$R_{\alpha\beta} = \overline{u'_\alpha u'_\beta} - \frac{1}{3}\delta_{\alpha\beta}\overline{u'_\gamma u'_\gamma} \tag{9}$$

The last three terms on the right side in (5), representing the small-scale motion, are the nonclosed terms that must be modeled by what is called the SGS model. Following, e.g., Deardorff (1970) [5], we make the simplification here that $C_{\alpha\beta} = 0$, and thus only $R_{\alpha\beta}$ remains to be modeled. The term $\overline{\overline{u}_\alpha \overline{u}_\beta}$ can be computed explicitly. For the numerical approach used here (i.e., one- point Gaussian quadrature and cell volume-averaging over an element) we have (McCallen, 1993 [6]).

$$L_{\alpha\beta} = 0 \tag{10}$$

The weak forms obtained via (3) and (4) for the domain Ω are [8]

$$\int_\Omega d\underline{x} w(\underline{x}) \frac{\partial \overline{u}_\alpha}{\partial x_\alpha} = 0 \tag{11}$$

and

$$\int_\Omega d\underline{x} v(\underline{x}) \{\frac{\partial \overline{u}_\alpha}{\partial t} + \frac{\partial}{\partial x_\beta}(\overline{u}_\alpha \overline{u}_\beta - \overline{\tau}_{\alpha\beta})\} = 0 \tag{12}$$

where $v(\underline{x})$ and $w(\underline{x})$ are appropriate sets of test functions. Integrating the stress term in (12) by parts and applying the divergence theorem, we arrive at the final weak form

$$\int_\Omega d\underline{x}\Big[v(\underline{x})(\frac{\partial \overline{u}_\alpha}{\partial t} + \frac{\partial}{\partial x_\beta}\overline{u}_\alpha \overline{u}_\beta) + \nu\frac{\partial \overline{u}_\alpha}{\partial x_\beta}\frac{\partial v}{\partial x_\beta} - \overline{P}\frac{\partial v}{\partial x_\alpha} - R_{\alpha\beta}\frac{\partial v}{\partial x_\beta}\Big] = \int_{\partial\Omega} dA v(\underline{x}) f_\alpha \tag{13}$$

where

$$f_\alpha = n_\beta \overline{\tau}_{\alpha\beta} \tag{14}$$

is the pseudo-stress applied on the domain boundary $\partial\Omega$. It is introduced as a natural boundary condition on the boundary surface $\partial\Omega$, where n_α is the unit vector normal to the surface pointing outward. In this formulation, the natural boundary conditions include the small-scale motion.

The solutions $\overline{u}_\alpha$ and $\overline{P}$ are expanded into appropriate (global) basis functions $\Phi_j(\underline{x})$ and $\Psi_j(\underline{x})$ as follows:

$$\overline{u}_\alpha^h(\underline{x},t) = \sum_{j=1}^{N} \overline{u}_\alpha^j(t)\Phi_j(\underline{x}) \tag{15}$$

$$\overline{P}^h(\underline{x},t) = \sum_{j=1}^{M} \overline{P}^j(t)\Psi_j(\underline{x}) \tag{16}$$

where N is the total number of velocity basis functions and M is the total number of pressure basis functions. The functions Φ_j and Ψ_j are linearly independent piecewise polynomial basis functions, which define the spatial variation of the solutions. The superscript h signifies that $\overline{u}_\alpha^h$ and $\overline{P}^h$ are the approximate weak solutions on a discretization of the computational domain Ω with characteristic element size h. These approximate solutions are well-defined at all points in the flow field, not just at discrete grid points as with finite difference schemes.

Substituting the expansions (15) and (16) into (11) and (13) and setting $v(\underline{x}) = \Phi_j(\underline{x})$ and $w(\underline{x}) = \Psi_j(\underline{x})$ (i.e., the Galerkin finite element method (GFEM)), we obtain

$$\Big(\int_\Omega d\underline{x}\Psi_i \frac{\partial \Phi_j}{\partial x_\alpha}\Big)\overline{u}_\alpha^j = 0 \tag{17}$$

and

$$\Big(\int_\Omega d\underline{x}\Phi_i\Phi_j\Big)\frac{\partial \overline{u}_\alpha^j}{\partial t} + \Big(\overline{u}_\beta^k \int_\Omega d\underline{x}\Phi_i \frac{\partial}{\partial x_\beta}\Phi_j\Phi_k\Big)\overline{u}_\alpha^j + \Big(\int_\Omega d\underline{x}\nu \frac{\partial \Phi_i}{\partial x_\beta}\frac{\partial \Phi_j}{\partial x_\beta}\Big)\overline{u}_\alpha^j$$
$$-\Big(\int_\Omega d\underline{x}\Psi_j \frac{\partial \Phi_i}{\partial x_\alpha}\Big)\overline{P}^j - \Big(\int_\Omega d\underline{x}R_{\alpha\beta}\frac{\partial \Phi_i}{\partial x_\beta}\Big) = \int_{\partial\Omega} dA\Phi_i f_\alpha \tag{18}$$

where summation over repeated subscripts is implied. The form of the nonclosed SGS terms depends on the particular expression of the SGS model.

3 Subgrid-scale model

The closure model for $R_{\alpha\beta}$ is the Smagorinsky model [10] given by

$$R_{\alpha\beta} = -2\nu_T S_{\alpha\beta} \tag{19}$$

where the resolved strain rate is defined by

$$S_{\alpha\beta} = \frac{1}{2}\Big(\frac{\partial \overline{u}_\alpha}{\partial x_\beta} + \frac{\partial \overline{u}_\beta}{\partial x_\alpha}\Big) \tag{20}$$

The LES-viscosity is according to [8] given by

$$\nu_T = (C\triangle)^2(2S_{\alpha\beta}S_{\alpha\beta})^{\frac{1}{2}} \tag{21}$$

where C is a constant in the original Smagorinsky model. The values for C reported in the literature vary significantly (see the paper by Smagorinsky in [11]) with $C = 0.1$ being a typical value, which is used in the present case.

4 Numerical method

The present GFEM method is based on trilinear basis functions $\Phi_j(\underline{x})$ (unity on node j and zero on all other nodes) for velocity and piecewise constant basis functions $\Psi_j(\underline{x})$ (unity on element j and zero on all other elements) for the pressure defined on isoparametric quadrilateral elements (Gresho et al., 1984 [9]). The number of velocity modes (global expansion functions) N is then equal to the number of nodes and the number of pressure modes M is equal to the number of elements. The weak Galerkin form (17) and (18) of mass and momentum balances contains only first derivatives for the velocity modes and zeroth derivatives for the pressure. Both are discontinuous but bounded across element boundaries for the present expansion functions, hence acceptable for GFEM. Given a discretization of the flow domain Ω in quadrilateral elements the weak forms (17) and (18) of mass and momentum balances lead to a system of matrix equations. This system can be written as

$$\mathbf{C}^T\overline{\mathbf{u}} = 0 \tag{22}$$

and

$$\mathbf{M}\frac{d}{dt}\overline{\mathbf{u}} + [\mathbf{K} + \mathbf{N}(\overline{\mathbf{u}})]\overline{\mathbf{u}} + \mathbf{C}\overline{\mathbf{P}} = \mathbf{F} \tag{23}$$

The matrix $\mathbf{C}$ in the mass balance (22) is assembled using

$$c_{ij}^{(\alpha)} = -\int_{\Omega} d\underline{x}\Psi_j\frac{\partial\Phi_i}{\partial x_\alpha} \tag{24}$$

and

$$C_{Ij} = c_{i,j}^{(\alpha)}$$

where the index $I(i,\alpha)$ (ranging over all nodes and all directions) in the matrix $\mathbf{C}$ and the solution vector $\overline{\mathbf{u}}$ is uniquely determined by the nodal index i and the direction α, the index j ranges over all elements. The relation $I(i,\alpha)$ is set up for book keeping purposes in the solution procedure for a given discretization of the flow field. The mass matrix $\mathbf{M}$ is defined by

$$M_{IJ} = \delta_{\alpha\beta}\int_{\Omega} d\underline{x}\Phi_i\Phi_j \tag{25}$$

where the indices $I(i,\alpha)$ and $J(j,\beta)$ have been defined above. The viscous and the LES terms in (18) generate the matrix $\mathbf{K}$ given by

$$K_{IJ} = \int_{\Omega} d\underline{x}\left\{\delta_{\alpha\beta}(\nu+\nu_T)\frac{\partial\Phi_i}{\partial x_\gamma}\frac{\partial\Phi_j}{\partial x_\gamma} + \nu_T\frac{\partial\Phi_j}{\partial x_\alpha}\frac{\partial\Phi_i}{\partial x_\beta}\right\} \tag{26}$$

The LES viscosity ν_T defined by (21) is determined by the resolved strain rate, hence it is constant within an element for the present choice of trilinear expansion functions $\Phi_i(\underline{x})$. The nonlinear convective terms are treated using the concept of centroid convection velocity introduced by Gresho et al. (1984) [9], where the resolved velocity in an element e is approximated by the value

$$\overline{u}_{\alpha,e} \tilde{=} \sum_{k=1}^{N_e}\overline{u}_\alpha^k\Phi_k(\underline{x}^c) \tag{27}$$

constant within element e, where N_e denotes the number of nodes per element and $\underline{x}^c$ the centroid location of element e. The computation of the elements of matrix $\mathbf{N}$

$$N_{IJ} = \delta_{\alpha\beta}\overline{u}_\gamma^k\int_{\Omega}\Phi_i\Phi_k\frac{\partial\Phi_j}{\partial x_\gamma} \tag{28}$$

can be considerably simplified with this approach with significant gain in speed. The vector $\mathbf{F}$ on the right side of (23) contains the natural boundary conditions (14). The entries are given by

$$F_I = \int_{\partial\Omega} dAx\Phi_i f_\alpha \tag{29}$$

where $I(i,\alpha)$ has been defined above.

The solution method for the matrix equations (22) and (23) is based on the discrete Poisson equation for the pressure, which follows from the divergence of the discrete momentum balance (23) and the discrete mass balance (22). This amounts to multiplying (23) with $\mathbf{C}^T\mathbf{M}^{-1}$ leading to

$$-\mathbf{C}^T\mathbf{M}^{-1}\mathbf{C}\overline{\mathbf{P}} = \mathbf{C}^T\mathbf{M}^{-1}[(\mathbf{K}+\mathbf{N}(\overline{\mathbf{u}}))\overline{\mathbf{u}} - \mathbf{F}] \tag{30}$$

where $\mathbf{C}^T\mathbf{M}^{-1}\mathbf{C}$ is an approximation of the Laplace operator. The system of equations to be solved is, therefore, given by (23) and (30). Furthermore, the concept of lumped mass matrix is employed to reduce the computational cost. The Euler time integration scheme is applied to (23) and the balancing tensor diffusivity and hour-glass correction techniques are used to improve the accuracy and stability of the scheme (Gresho et al., 1984 [9]).

5 Boundary conditions

The boundary conditions at the entrance section are straightforward, since the velocity is specified. The exit section is handled by setting the pseudo-stress $f_\alpha = 0$ in the natural boundary conditions contained in the right side vector $\mathbf{F}$. The treatment of the fixed wall boundaries is a challenge. The velocity has to satisfy the noslip condition at the wall. This requires very fine discretization of the near wall region and a modification of the LES viscosity to account for the fact that the stresses approach zero as the wall is approached. Piomelli et al. (1987) [7] provide a detailed review of wall models used in LES simulations of non-separating turbulent flows. However, non-separating flows give little indication concerning the behaviour in the region near separation and reattachment points or lines. It is unlikely (Reynolds, 1989 [12]) that the law of the wall holds in this type of region. A plausible option is then to use the LES viscosity all the way to the wall without detailed resolution of the near wall region. This approach is used in the present case.

6 Problem Definition

Our test problem was the backward-facing step at the Reynolds number of 10,000 based on the inlet velocity and two times the inlet channel height. The problem geometry was nondimensionalized using a channel of unit height with a step height of 0.5 and a total channel length of ten. For the three-dimensional (3-d) calculations we chose an out-of-plane depth of one channel height. Periodic boundary conditions were specified on the out-of-plane (lateral) boundaries. The computational domain begins at the step with a uniform velocity profile of unity at the entrance. At the wall, we used no-penetration and no-slip boundary conditions, and at the outflow, homogeneous natural boundary conditions. The Smagorinsky model constant was set to $C = 0.1$.

7 Results

The 3-d time-averaged LES results were validated by comparison to both a 3-d high-resolution run with no LES model, and to the experimental results of Armaly et al. [13]. Table 1 lists the predicted and measured reattachment positions (step-height normalized) for the step recirculation zone. Our figures demonstrate the ability of LES to represent the large-scale and complicated vortex shedding phenomena in flow over the backward-facing step.

LES results were obtained for several different mesh densities and configurations. The 3-d LES results we report here are with the coarsest graded mesh of 45,056 elements. A 6 to 1 mesh grading was used for the 6 elements closest to the top and bottom walls with $\triangle y_{min} = 0.0047$. In the z-direction (out-of-plane), the mesh is uniform with $\triangle z = 0.0625$. A stable time step of 0.005 corresponded to a stationary time history of total kinetic energy.

The 3-d high-resolution case of the test problem is calculated with the same code, but without an SGS model. We hesitate to refer to this as a direct numerical simulation (DNS), but do so as abbreviation to indicate that the LES model is turned off. This high-resolution run using a 187,392 element mesh and a time step of 0.005 resolves significantly more scales than the LES run, but it does not resolve all scales.

Armaly's experimental results indicate that the reattachment position is not changing in the fully turbulent regime (i.e. $Re > 6600$) thus his measured results can be used for comparison to our simulations. The comparison of the reattachment positions obtained for the DNS low and high resolution meshes with Armaly's data shows improvement as the mesh is refined (see Table 1). Our LES run (low resolution mesh) provided the closest match to the experimental data, showing a difference of less than 4%.

In order to validate our Smagorinsky SGS model, we reproduced the 2-d results reported by McCallen et al., 1993 [8] with a mesh of 7,808 elements (Fig.1a). That result agreed with a DNS on a 100,000 element mesh which resolved at least ten Kolmogorov scales. Our present 3-d LES run shows (lateral vorticity component in Fig.1b) a complicated time-varying flow as with the 2-d LES in Fig.1a. However, the 3-d simulation displayed vortices shedding off the recirculation zone and the midsection of the top wall, not at the step, as in the 2-d simulation. It appears that the restriction to two dimensions produces Kelvin-Helmholtz type shear instability at the step leading to large structures of the rolling vortex type. This striking difference between 2-d and 3-d remains to be explored.

The 3-d simulation goes through an initial 2-d evolution, until the first vortex reaches the outflow boundary and trips the flow to become 3-d (Fig.1b). The isobaric surfaces, shown in the upper views of Fig.2, indicate the 2-d character of the flow in the early phase of the evolution, and they also show 3-d disturbances that start to grow below the step in the recirculation zone. Disturbances propagate downstream and produce the smaller-scale turbulent features observed past the reattachment region. However, the large structures upstream and near the upper wall remain virtually 2-d. The flow does not evolve to an exact periodic solution as in 2-d, but retains some periodic characteristics.

Table 1. Reattachment positions for 3-d simulations and experiment

Run description	Number of elements	Reattachment position
LES	45,056	8.24
DNS (high resolution mesh)	187,392	9.18
DNS (low resolution mesh)	45,056	6.18
Armaly et al. (1983)	experiment	7.95

We see random behavior, with no repeated discernible patterns, in the velocity time histories shown in Fig.3. These velocity components are sampled at a point in the flow just downstream of the recirculation zone, in our LES run. It is difficult to recognize the flow structure from these complicated time histories by visual inspection. Therefore, we obtained the power spectra of these signals for further analysis.

Power spectrum results for the velocities are given in Fig.4 and show a number of dominant frequencies. It is seen that the velocity components in different directions have different dominant frequencies, which is not inconsistent with the Navier-Stokes equations. The u-power spectrum has two dominant peaks near the dimensionless frequency 0.3, whereas the power spectra for the wall normal v and the lateral w velocity components do not. This behavior is explained by a strong oscillatory motion in the longitudinal direction, but not in the normal or lateral direction, near this point.

8 Conclusions

The present contribution shows that the finite element method can be combined with the LES approach and successfully applied to complicated flow problems in the turbulent regime.

Past work showed that 2-d LES/FEM produced an accurate simulation of the large-scale flow using only 7,808 elements in comparison to 100,000 elements needed for DNS. In this present 3-d work, an accurate LES simulation was obtained with only 45,056 elements in contrast to 187,392 elements in a high-resolution run (DNS). The main conclusion from the comparison of 2-d and 3-d simulations is that the vortices shed from the step in 2-d and from the recirculation zone in 3-d. This significant difference in flow characteristics shows the importance of using 3-d simulations.

We used time-averaged results to compare different numerical runs with experimental data. The reattachment length from our 3-d LES run agrees to within 4% with the experiment.

9 Acknowledgement

Funding for this collaborative effort between LLNL and UC Davis was through a grant from the Center for Advanced Fluid Dynamics Applications (CAFDA) at LLNL. This work was performed under the auspices of the U.S. Department of Energy by Lawrence Livermore National Laboratory under Contract W-7405-Eng-48.

10 References

[1] N. Kondo, N. Tosaka, and T. Nishimura, Finite Element Analysis for Turbulent Flows-Elastic Shell Interaction, Proceedings from Sixth International Symposium on Finite Element Methods in Flow Problems, 16-20 June 1986, Antibes, France (1986) 177-181.

[2] A. N. Findikakis, J. B. Franzini, and R. L. Street, Simulation of Stratified Turbulent Flows in Closed Water Bodies Using the Finite Element Method, Proceedings from Finite Elements in Water Resources Conference, July 1978, London, England (1978) 3/23-44.

[3] A. N. Findikakis and R. L. Street, Numerical Simulation of Turbulent Stratified Flows in Surface Water Impoundments, Proc. of the Spec. Conf. on Comput. and Phys. Model in Hydraul. Eng., Chicago, Illinois, August 6-8, 1980, Published by ASCE, New York, NW (1980) 249-260.

[4] D. Kwak, W. C. Reynolds, and J. H. Ferziger, Three Dimensional Time Dependent Computation of Turbulent Flow, Report TF-5, Dept. of Mech. Engr., Stanford University (1975).

[5] J.W. Deardorff, A Numerical Study of Three-Dimensional Turbulent Channel Flow at Large Reynolds Numbers, J. Fluid Mech. **41**, 1970, pp.453-480.

[6] R. McCallen, Large-Eddy Simulation of Turbulent Flow Using the Finite Element Method, University of California, Davis, Ph.D. Thesis (1993).

[7] U. Piomelli, J. H. Ferziger, and P. Moin, Models for Large-Eddy Simulation of Turbulent Channel Flows including Transpiration, Rept TF-32, Dept. of Mech. Engr., Stanford University (1987).

[8] R. McCallen, P. Gresho, J. Leone, and W. Kollmann, Large-Eddy Simulation Using the Finite Element Method, Proc. of the 1994 ASME Fluids Engineering Summer Meeting, Lake Tahoe, NV, June 19-23, 1994.

[9] P. M. Gresho, S. T. Chan, R. L. Lee, and C. D. Upson, A Modified Finite Element Method for Solving the Time-Dependent Incompressible Navier-Stokes Equations, Part 1: Theory, International Journal of Numerical Methods in Fluids, Vol. 4 (1984), pp. 557-598.

[10] J. Smagorinsky, General Circulation Experiments with the primitive Equations, I. the Basic Experiment, Monthly Weather Review, vol. **91**, (1963), pp. 99-164.

[11] B. Galperin and S.A. Orszag (eds.), Large Eddy Simulation of Complex Engineering and Geophysical Flows, Cambridge University Press, (1993).

[12] W.C. Reynolds, The potential and limitations of Direct and Large Eddy Simulations, in Whither Turbulence? or Turbulence at the Crossroads (J.L. Lumley ed.), Lecture Notes in Physics vol. **357**, Springer V., pp. 245-272.

[13] B.F. Armaly, F. Durst, J.C.F. Periera and B. Schönung, Experimental and Theoretical Investigation of Backward Facing Step Flow, J. Fluid Mech., **127**, pp.473-496.

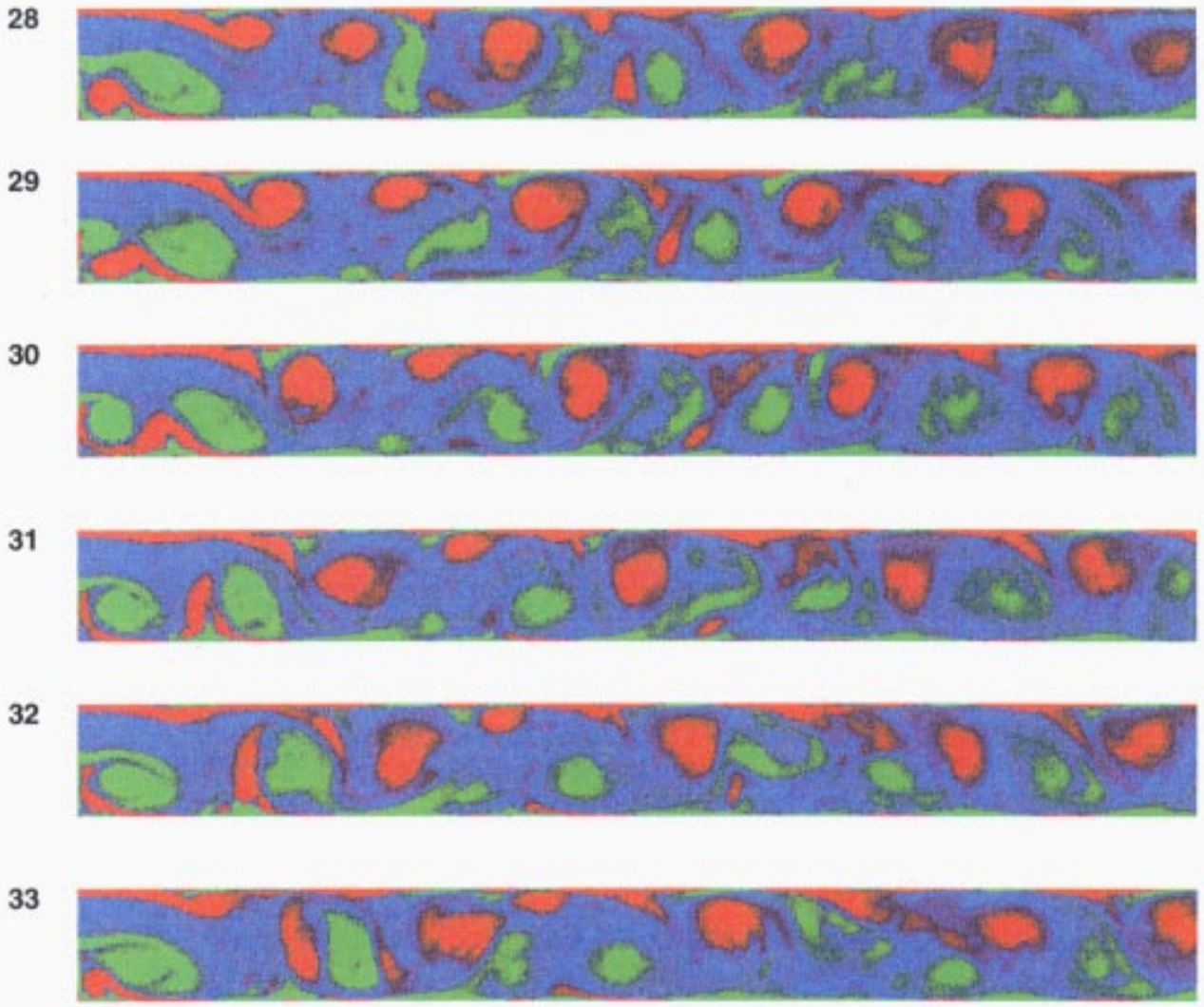

Fig.1a. Series of vorticity snapshots for two-dimensional LES simulation over 5 time units.

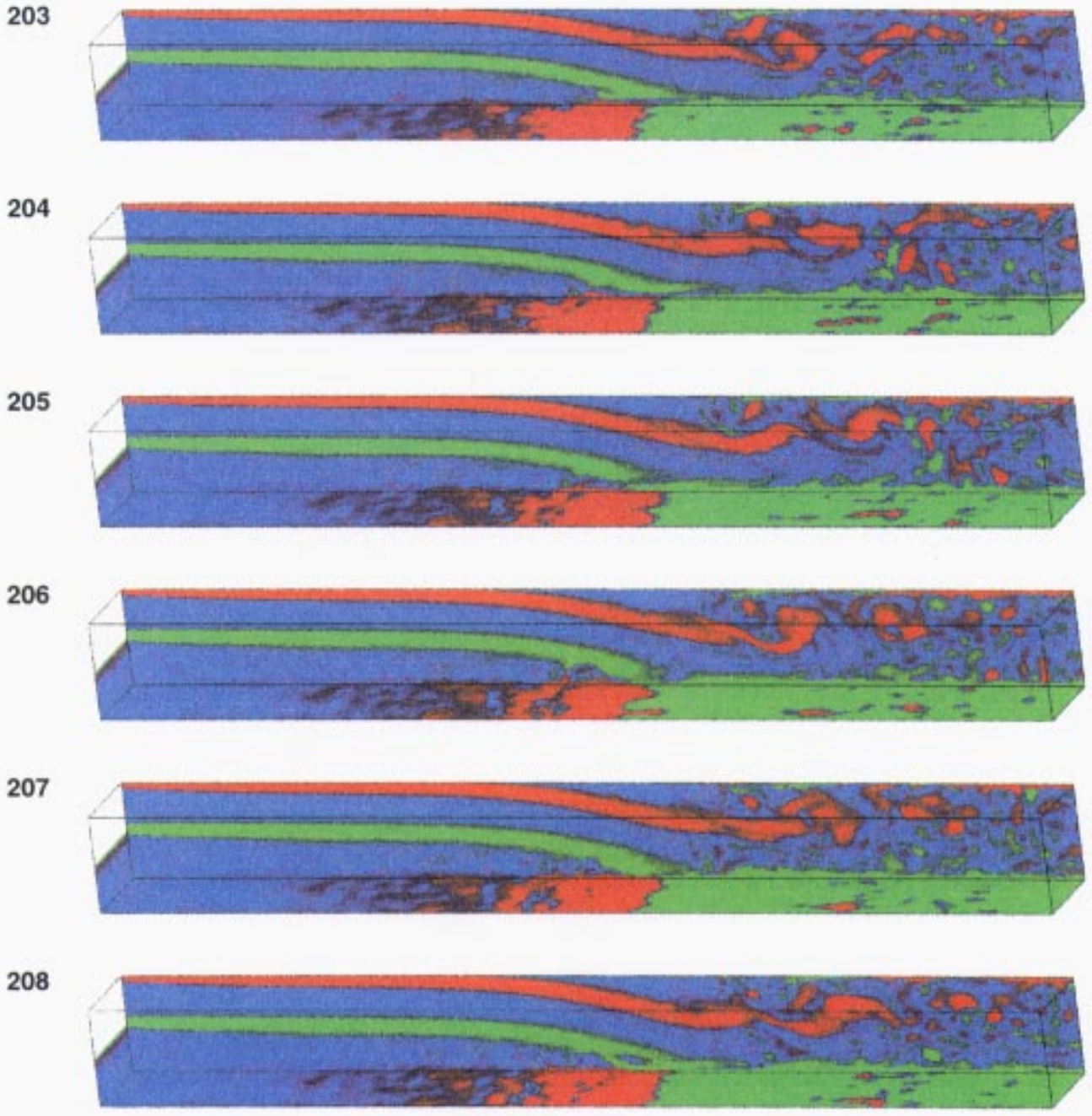

Fig.1b. Series of vorticity snapshots for three-dimensional LES over 5 time units.

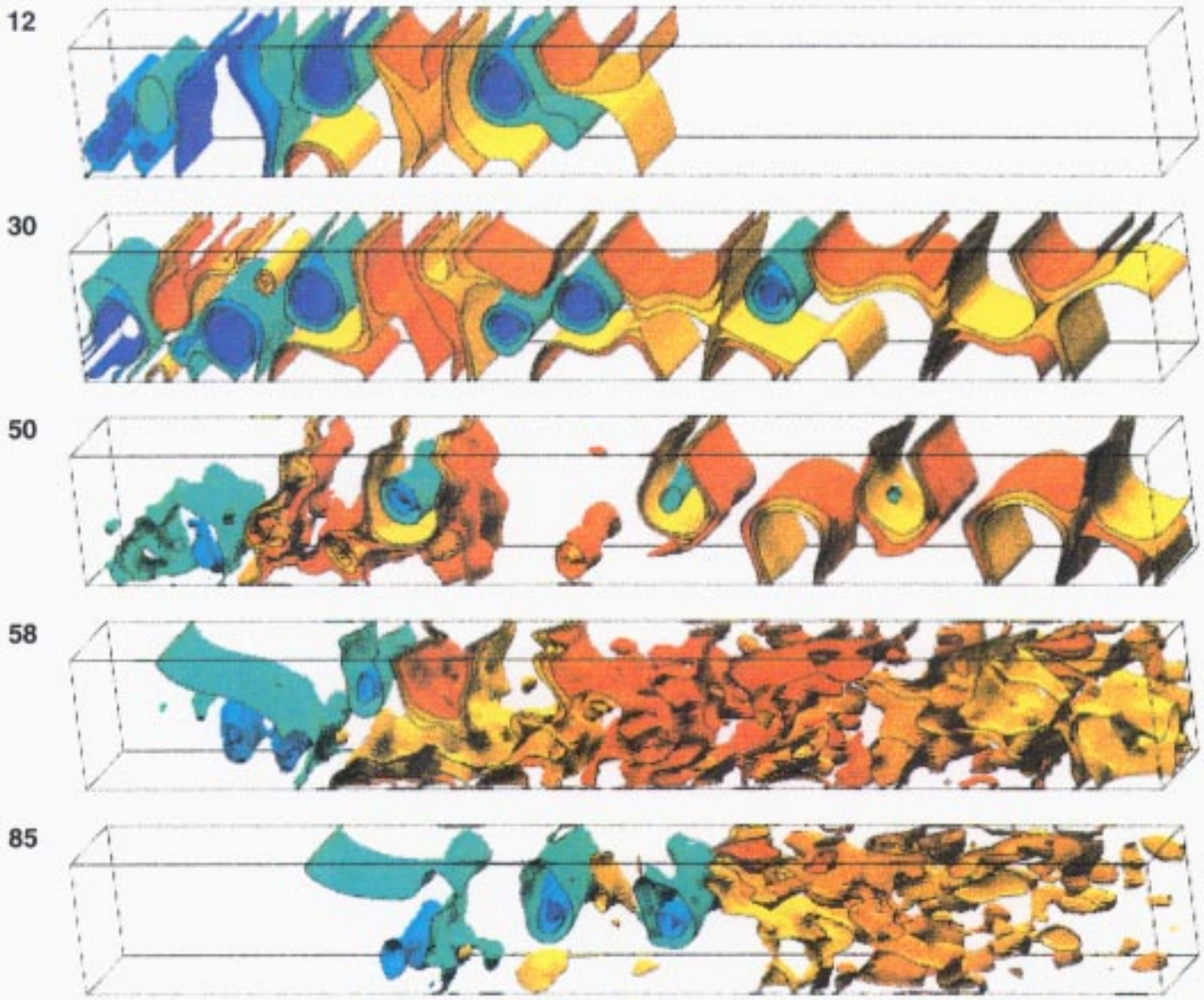

Fig.2. Time series of pressure iso-surfaces showing the flow evolution from start-up to a fully developed three-dimensional flow. Numbers indicate non-dimensional time units.

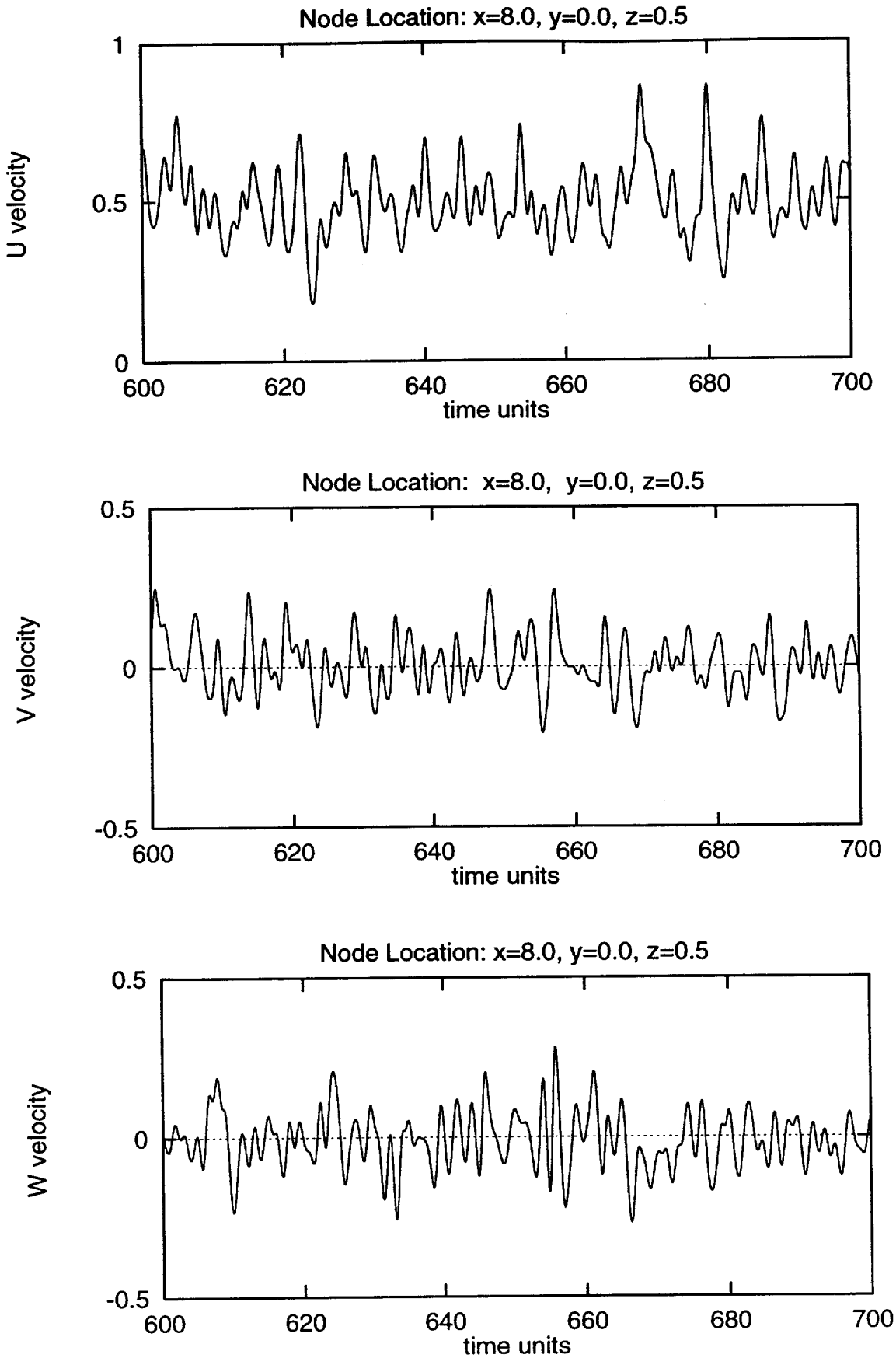

Fig.3. Time histories at $(x, y, z) = (8.0, 0.0, 0.5)$ for the three velocity components for the LES simulation.

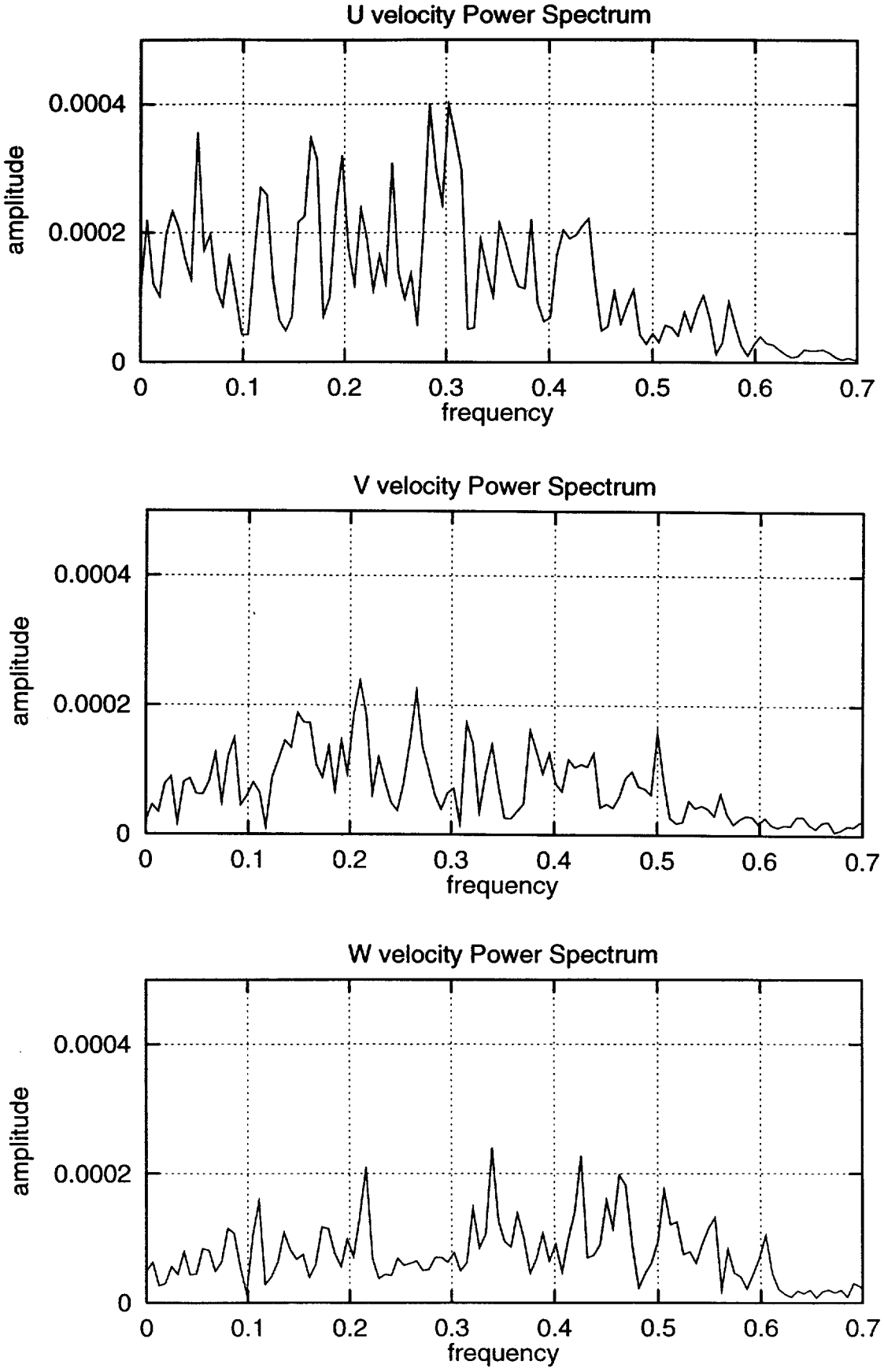

Fig.4. Power spectra for the time histories in Figure 3.

Technical Information Department • **Lawrence Livermore National Laboratory**
University of California • Livermore, California 94551